Supplementary Figure S1

Supplementary Figure S1 – Methylation profiling of the infant cohort. t-statistic based stochastic neighbor embedding (t-SNE) projection of a combined methylation dataset comprising the initial, pathognomic fusion-excluded set of the present study (n=198, circled) plus a reference set of entities and subtypes from across the spectrum of CNS malignancies (n=3949). The first two projections are plotted on the x and y axes, with samples represented by dots colored by subtype according to the key provided.

Supplementary Figure S2

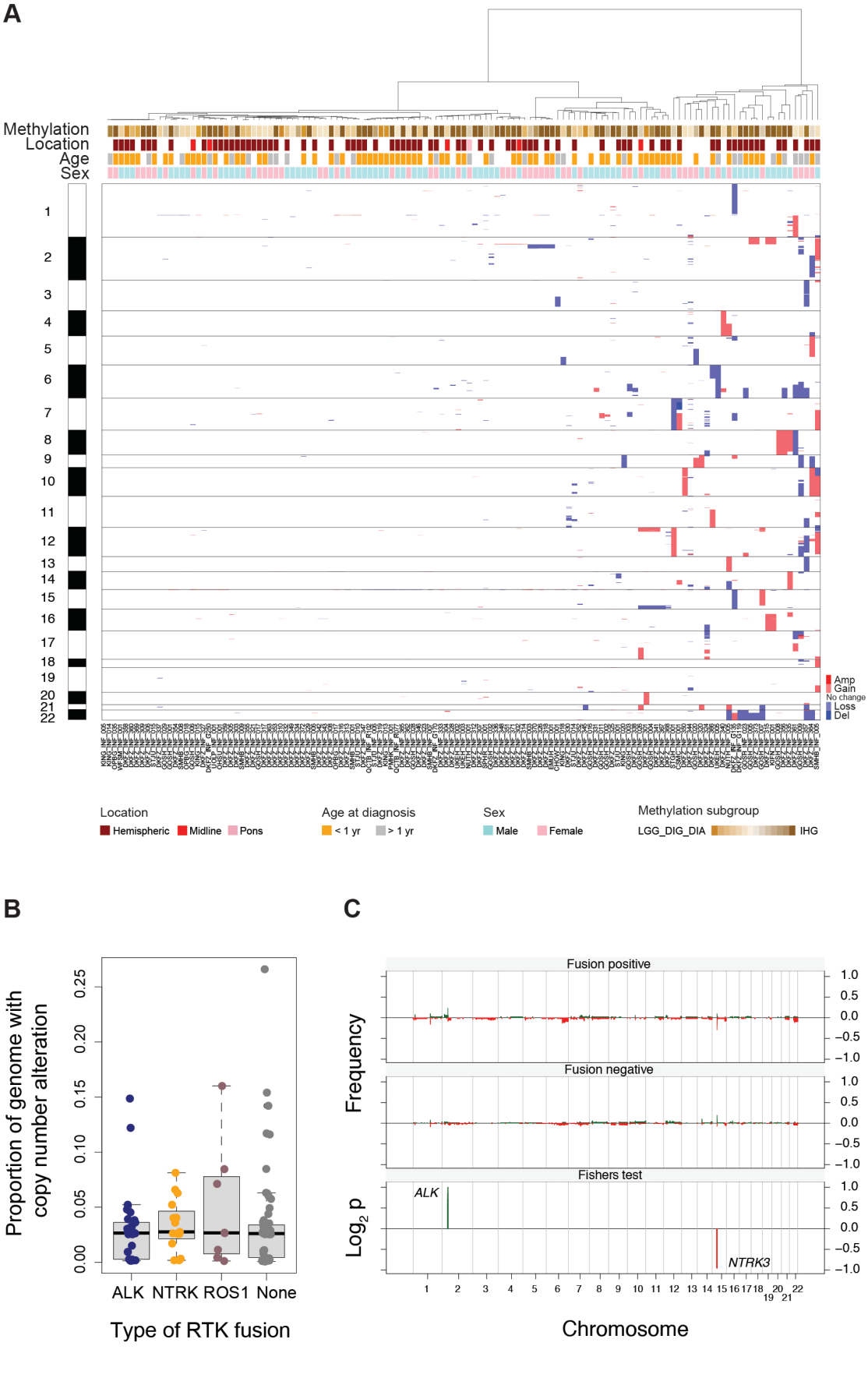

Supplementary Figure S2 – DNA copy number profiling of the intrinsic set. (A) Heatmap representation of segmented DNA copy number for 130 intrinsic samples of infant glioma profiled on the Illumina 450kor EPIC BeadArray platform (dark red, amplification; red, gain; dark blue, deletion; blue, loss). Samples are arranged in columns clustered by contiguous categorical copy number states based upon log ratio thresholds of ±0.1 for gain/loss and ±0.5 for amplification and deletion. Clustering used Euclidean distance and a ward algorithm. Clinicopathological and molecular annotations are provided as bars according to the included key. (B) Boxplot of copy number changes separated by RTK fusion type. The thick line within the box is the median, the lower and upper limits of the boxes represent the first and third quartiles, and the whiskers 1.5x the interquartile range. (C) Frequency histogram (y axes) of copy number changes plotted according to chromosomal location (x axes) for fusion-positive (top) and fusion-negative (middle) cases. Bottom - $\log_2$ p values derived from a Fishers test comparison between fusion-positive and -negative cases are plotted against chromosomal location (x axis). Copy number gains are plotted in green, losses in red.

Supplementary Figure S3

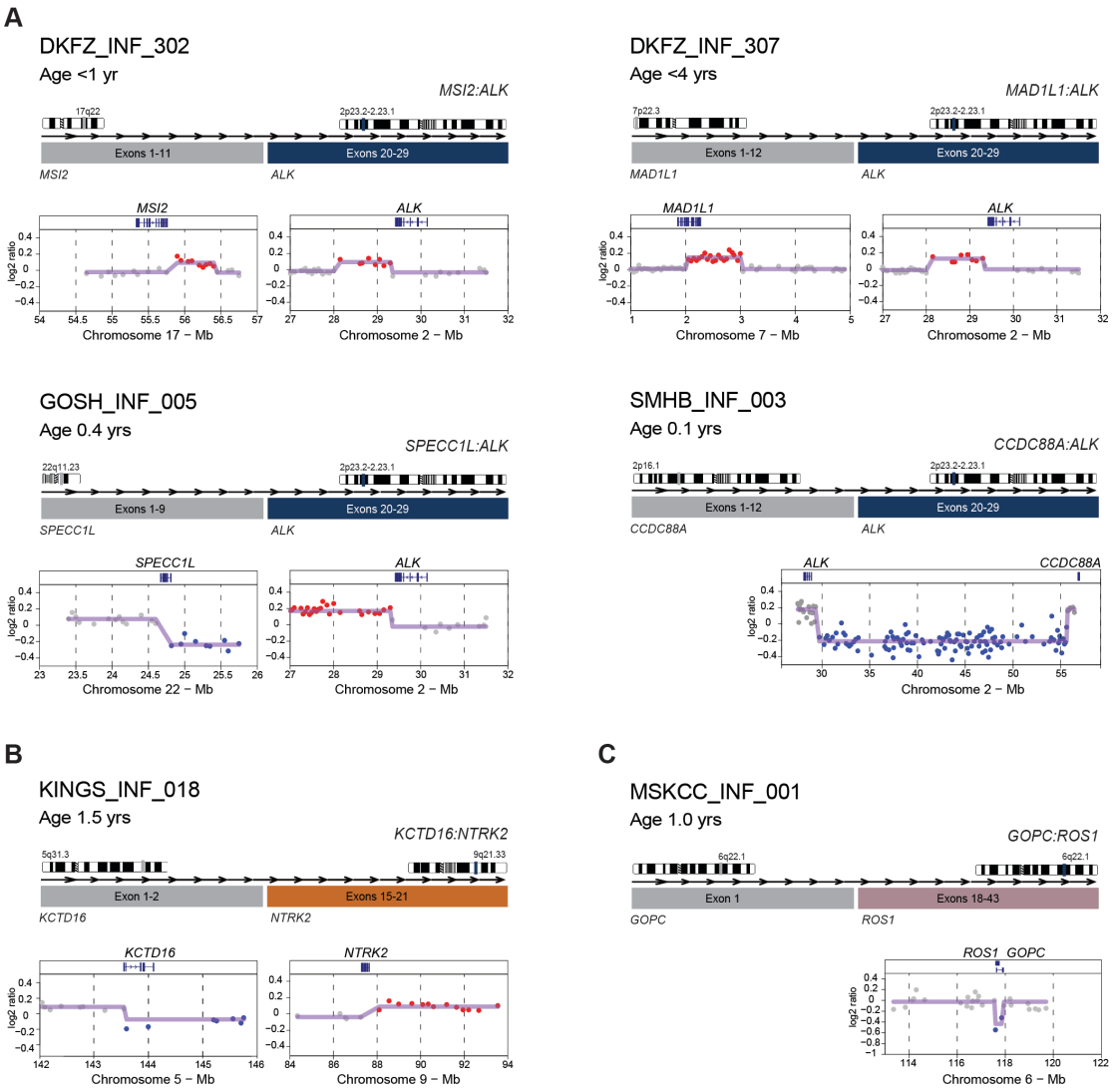

Supplementary Figure S3 – Copy number-associated fusion genes in infant gliomas. (A) *ALK*. Cartoon representation of the fusion structure, with copy number plots (log2 ratio, y axis) for chromosomal regions spanning the breakpoints (x axis) underneath. Points are colored red for copy number gain, blue for loss, and grey for no change. The smoothed values are overlaid by the purple line. (B) *KCTD16:NTRK2*. Cartoon representation of the fusion structure, with copy number plots (log2 ratio, y axis) for chromosomal regions spanning the breakpoints (x axis) underneath. Points are colored red for copy number gain, blue for loss, and grey for no change. The smoothed values are overlaid by the purple line. (C) *GOPC:ROS1*. Cartoon representation of the

fusion structure, with copy number plots (log2 ratio, y axis) for chromosomal regions spanning the breakpoints (x axis) underneath. Points are colored red for copy number gain, blue for loss, and grey for no change. The smoothed values are overlaid by the purple line.

Supplementary Figure S4

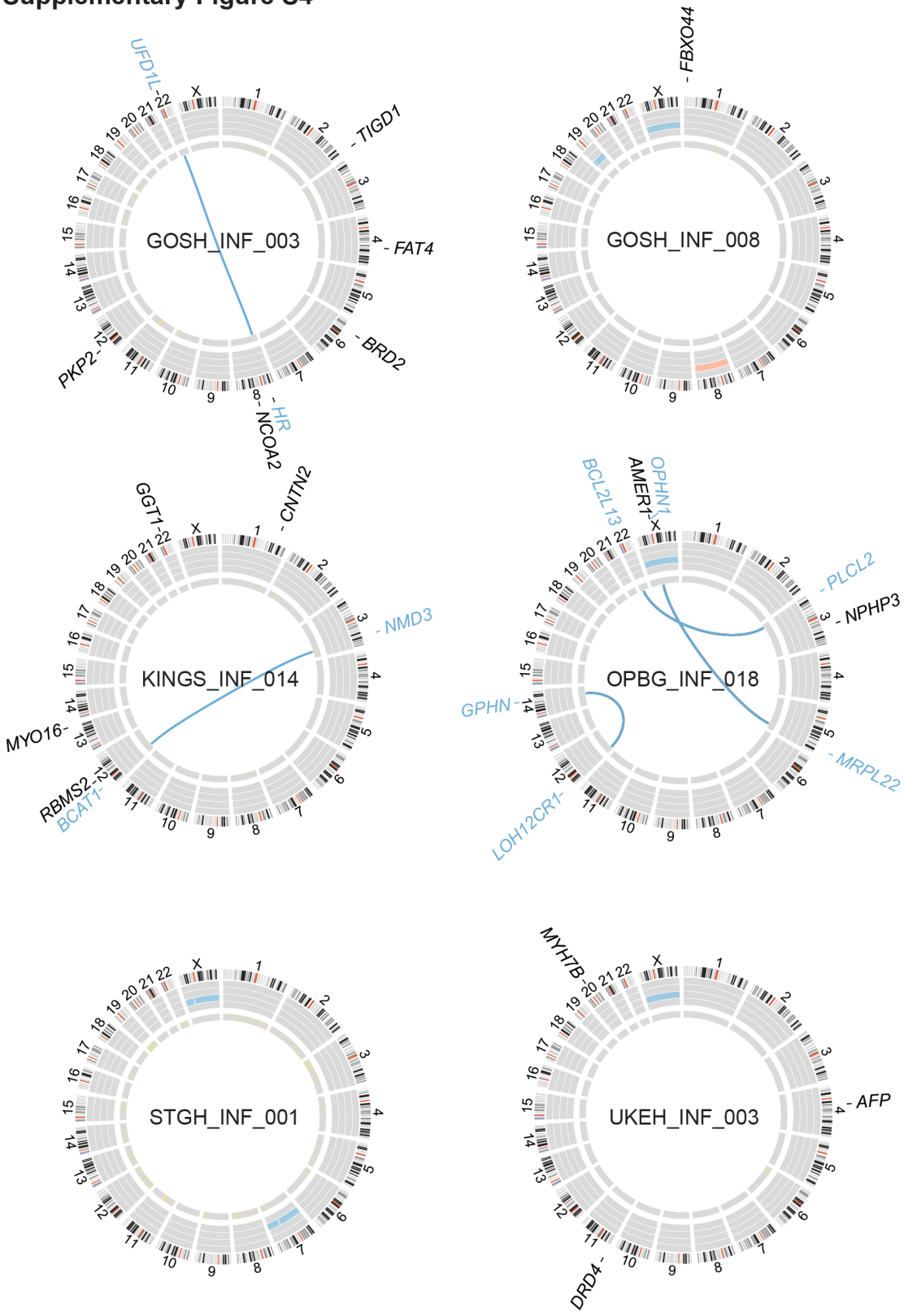

Supplementary Figure S4 – Whole genome sequencing of fusion-negative infant glioma cases. In each case, Circos plots provide somatic SNVs and InDels on the outer ring, DNA copy number changes (dark red, amplification; red, gain; dark blue, deletion; blue, loss) and loss of heterozygosity (yellow) on the inner rings, and inter-chromosomal translocations (blue) inside the circle.

Supplementary Figure S5

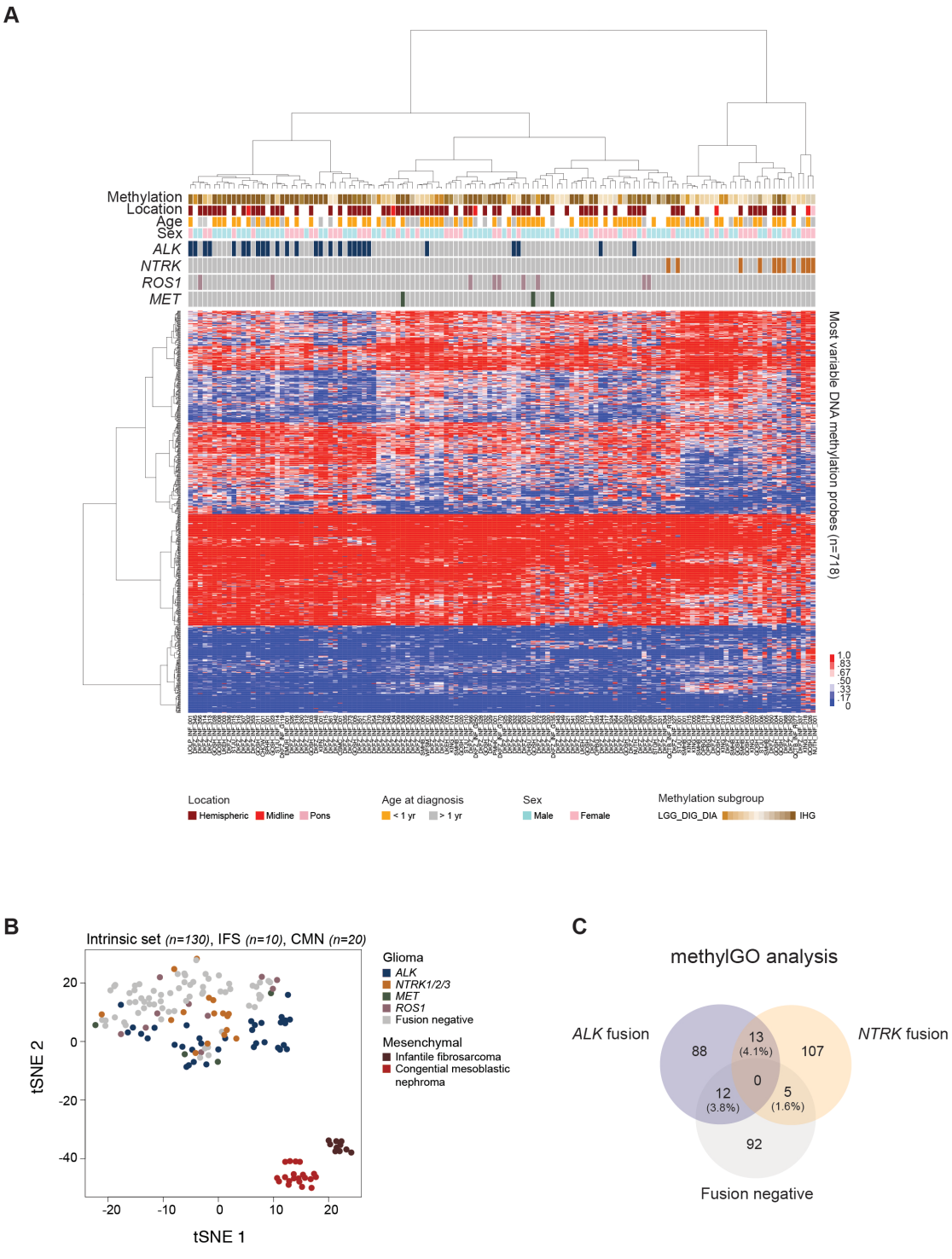

Supplementary Figure S5 – Methylation profiling of the intrinsic set on the basis of RTK fusions. (A) Hierarchical clustering and heatmap representation of beta values for 130 intrinsic samples profiled on the Illumina 450k or EPIC BeadArray platform (red, high; blue, low). Samples are arranged in columns clustered by the most variable 714

array probes across intrinsic subgroups. Clinicopathological and molecular annotations are provided as bars according to the included key. (B) t-statistic based stochastic neighbor embedding (t-SNE) projection of a combined methylation dataset comprising the intrinsic infant glioma set (n=130) as well as two *ETV6:NTRK3*-driven mesenchymal tumors, infantile fibrosarcoma (n=10) and congenital mesoblastic nephroma (n=20). The first two projections are plotted on the x and y axes, with samples represented by dots colored by subtype according to the key provided. (C) Pie chart showing overlap of significant gene ontology annotations of differentially methylated regions between *ALK*-fusion, *NTRK*-fusion and fusion-negative infant glioma cases.

Supplementary Figure S6

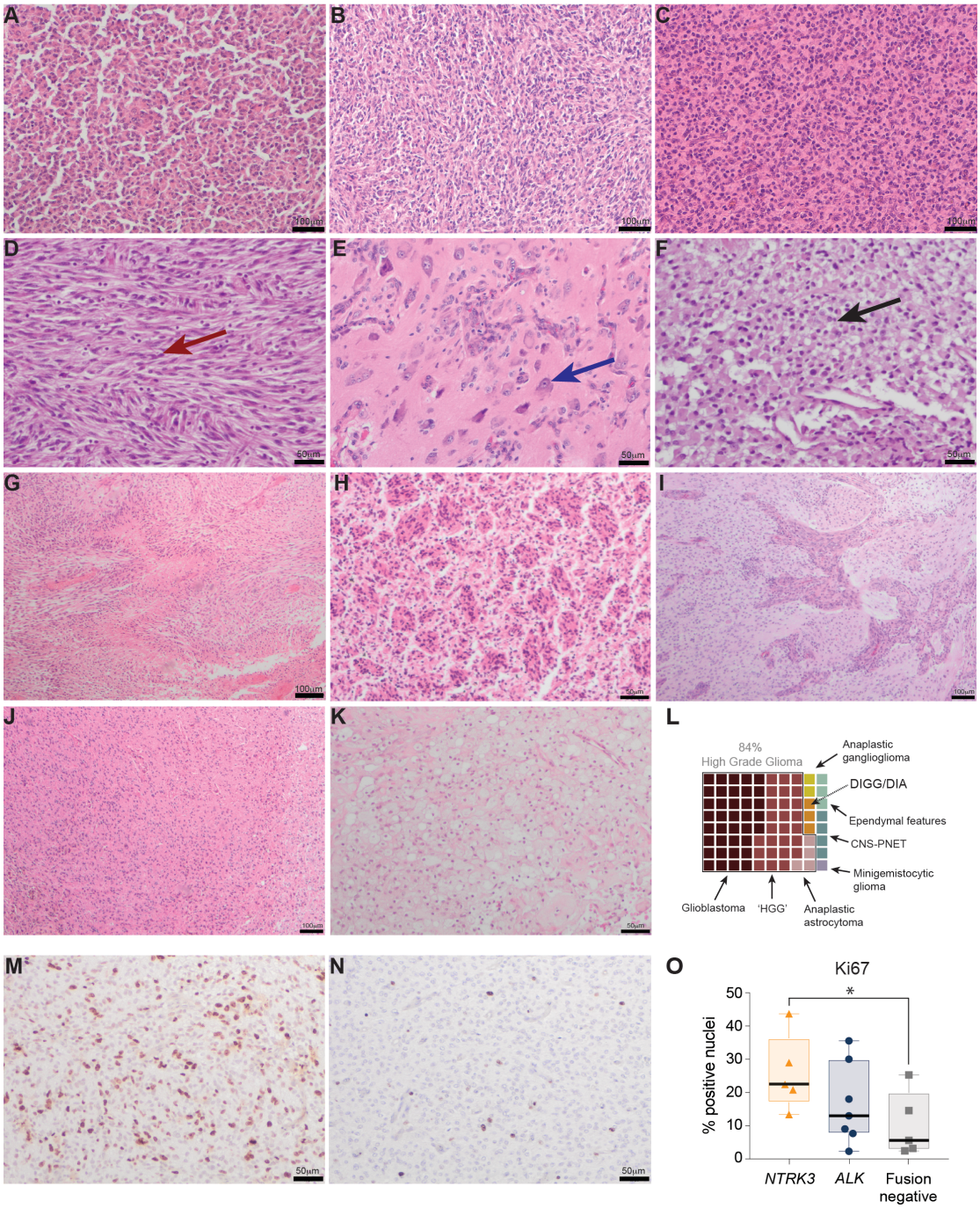

Supplementary Figure S6 – Histopathological assessment of IHG cases. (A-C) H&E images displaying examples of the high cellularity and uniform architecture of the IHG group. (D) The cytological appearances show more variation with some cases containing focal spindle shaped nuclei (red arrow). (E) Very occasionally ganglion cell differentiation is seen (blue arrow). (F) Some cases can show a gemistocyte-like

cytological appearance (black arrow). (G) High grade features including palisading necrosis are frequently seen. (H) H&E image showing a nodular architecture in an IHG case. (I) An IHG case displaying prominent nodularity and some microvascular proliferation. (J) An example of an IHG case which is less cellular and has a less uniform architecture. (K) Focal xanthomatous change in an IHG case. Scale bars are provided. (L) Plot representing the original diagnoses of IHG cases, colored and ordered according the labels provided. (M) Immunohistochemistry for Ki67 showing strong, frequent nuclear positivity. (N) Immunohistochemistry for Ki67 showing only isolated positive nuclei. Scale bars are provided. (O) Boxplot of Ki67 nuclear positivity in IHG cases by immunohistochemistry, separated by cases containing *NTRK3* fusions (orange), *ALK* fusions (dark blue) or fusion-negative (grey). The thick line within the box is the median, the lower and upper limits of the boxes represent the first and third quartiles, and the whiskers 1.5x the interquartile range. * $p<0.05$, t-test.

Supplementary Figure S7

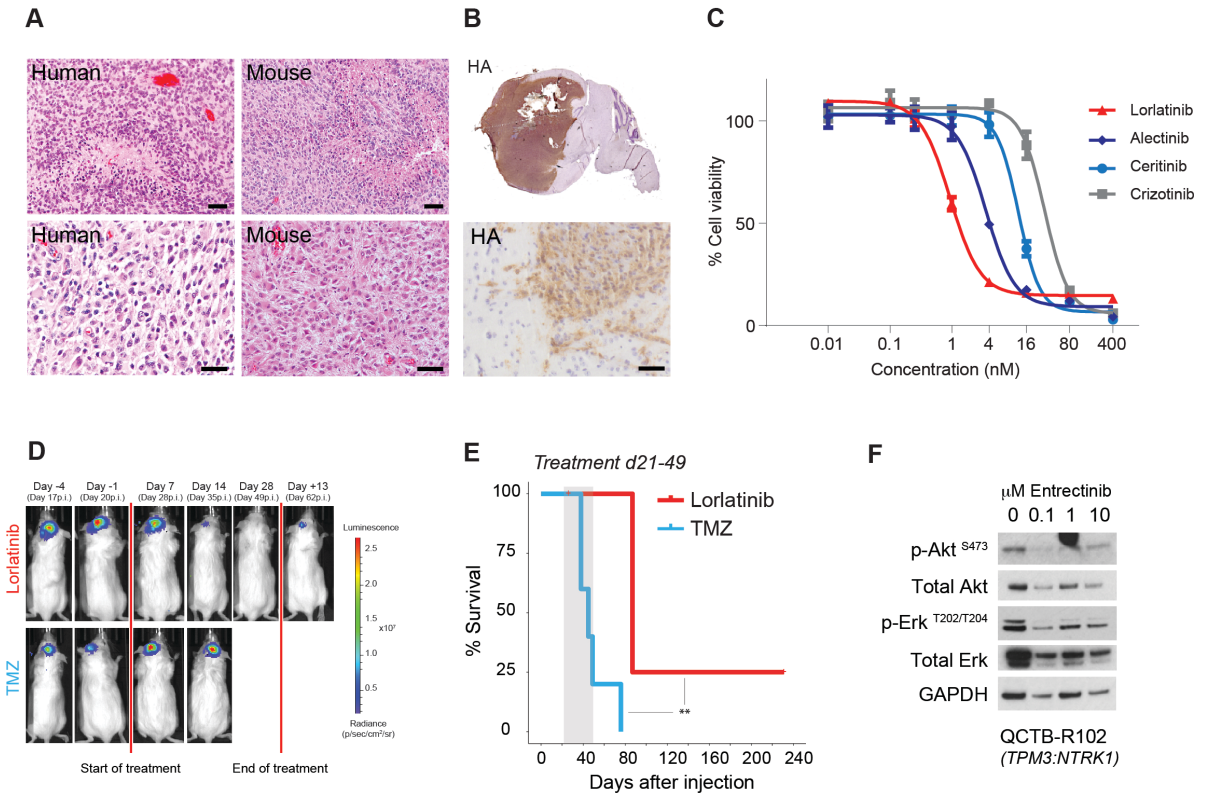

Supplementary Figure S7 – Fusion-driven models and clinical experience. (A) H&E staining of representative human ALK fusion-positive tumors and *PPP1CB:ALK* +/- *Cdkn2a*-ko IUE mice showing evidence of palisading necrosis (top) and clear astrocytic differentiation (bottom). (B) Whole-brain HA-tag staining of a representative *PPP1CB:ALK* + *Cdkn2a*-ko IUE mouse indicating expression of the ALK fusion transgene (top) and single tumor cells infiltrating into the normal brain parenchyma (bottom). (C) Primary cells derived from a *PPP1CB:ALK* fusion + *Cdkn2a*-ko mouse tumor display sensitivity to various targeted ALK inhibitors. (D) Effect of targeted ALK inhibition on growth of allografted *PPP1CB:ALK* only mouse tumor cells *in vivo*. p.i., post injection. (E) Targeted inhibition significantly prolonged the survival of *PPP1CB:ALK* only allografted mice compared with temozolomide. **, p<0.01. (F) Western blot analysis of phosphorylated and total Akt and Erk for QCTB-R102 cells (*TPM3:NTRK1*) treated with increasing concentrations of entrectinib.

Supplementary Figure S8

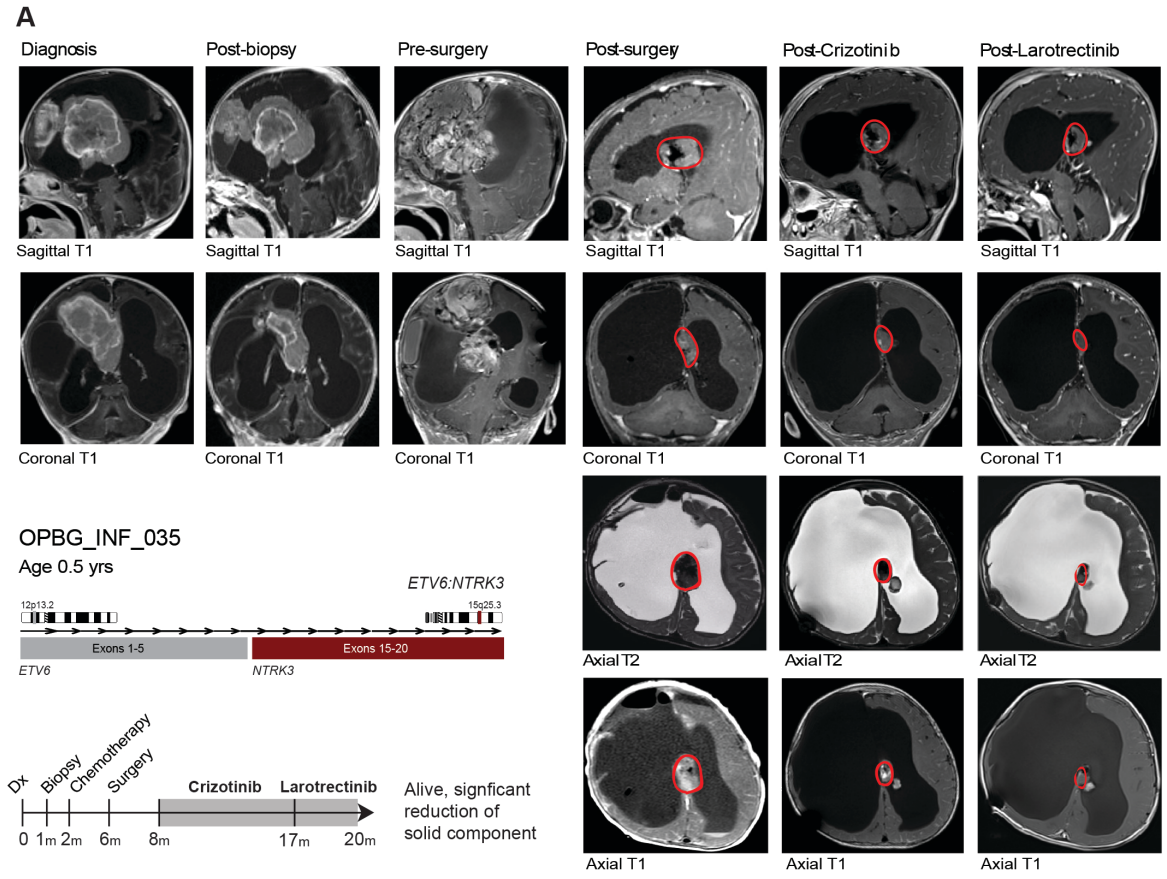

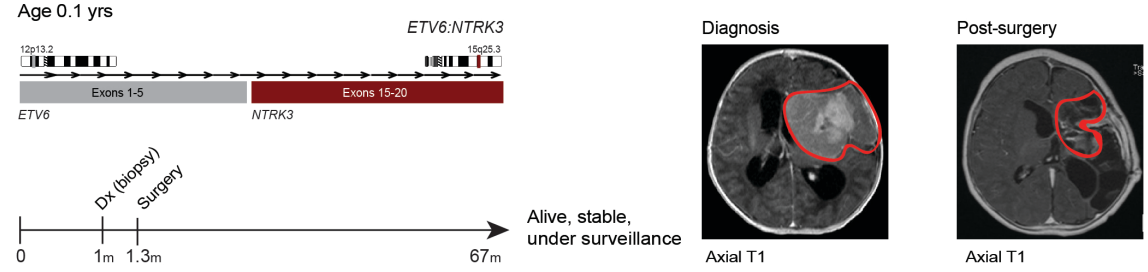

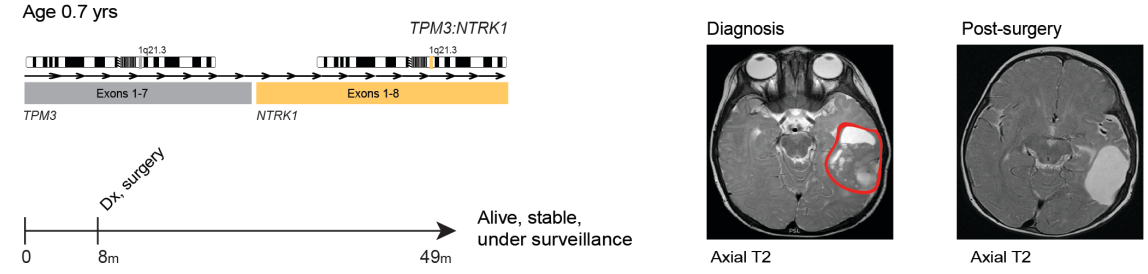

Supplementary Figure S8 – Clinical experience with NTRK-fusion cases. (A) Clinical history of OPBG_INF_035, with confirmed *ETV6-NTRK3* fusion. Timeline of clinical interventions is provided below, with Trk inhibitor treatment shaded in grey. Diagnosis, post-biopsy, pre/post-surgery, post-crizotinib and post-larotrectinib timepoints are provided, with sagittal and coronal T1 for all, and additionally axial T2 and T1 for post-surgery and Trk inhibitors, with tumor circled in red. (B) Clinical history of QCTB_INF_R077, with confirmed *ETV6-NTRK3* fusion. Timeline of clinical interventions is provided below. Diagnosis and post-surgery axial T1 MRI scans are provided, with tumor circled in red. (C) Clinical history of QCTB_INF_R102, with confirmed *TPM3:TRK1* fusion. Timeline of clinical interventions is provided below. Diagnosis and post-surgery axial T1 MRI scans are provided, with tumor circled in red.

Supplementary Tables

Supplementary Table S1 – Sample cohort. Clinicopathological and initial molecular profiling data of the full infant cohort (n=241).

Supplementary Table S2 – Methylation profiling. Heidelberg classifier v11b4 scores for the entire infant cohort, (n=241).

Supplementary Table S3 – Copy number analysis. Chromosomal gains and losses derived from methylation array analysis for the infant cohort, after quality control fail exclusions (n=231).

Supplementary Table S4 – Fusion gene analysis. List of candidate gene fusions, with platform for which evidence is derived, and validation where available (n=82).

Supplementary Table S5 – Differential methylation analysis. List of differentially methylated regions with associated statistics between *ALK*-fusion (n=36), *NTRK*-fusion (n=16) and fusion-negative (n=65) cases. Regions are annotated for genomic location, and relationship to gene and/or CpG island.

Supplementary Table S6 – Histopathological assessment. Architectural and cytological features of IHG cases, as well as Ki67 staining by immunohistochemistry (n=20).

Supplementary Table S7 – *In vitro* efficacy of targeted inhibitors. GI_{50} values for ALK and NTRK inhibitors tested against mouse and patient-derived cells.